Molecular Plant
Research Article

CellPress
PARTNER JOURNAL

Cytochrome *b*5 Reductase 1 Triggers Serial Reactions that Lead to Iron Uptake in Plants

Young Jun Oh[1], Hanul Kim[2], Sung Hee Seo[3], Bae Geun Hwang[4], Yoon Seok Chang[3], Junho Lee[2], Dong Wook Lee[1], Eun Ju Sohn[1], Sang Joon Lee[4], Youngsook Lee[1,2] and Inhwan Hwang[1,2,*]

[1]Division of Integrative Biosciences and Biotechnology

[2]Department Life Sciences

[3]Division of Environmental Science and Engineering

[4]Division of Mechanical Engineering
Pohang University of Science and Technology, Pohang 790-784, Korea

***Correspondence: Inhwan Hwang (ihhwang@postech.ac.kr)**

http://dx.doi.org/10.1016/j.molp.2015.12.010

ABSTRACT

Rhizosphere acidification is essential for iron (Fe) uptake into plant roots. Plasma membrane (PM) H^+-ATPases play key roles in rhizosphere acidification. However, it is not fully understood how PM H^+-ATPase activity is regulated to enhance root Fe uptake under Fe-deficient conditions. Here, we present evidence that cytochrome *b*5 reductase 1 (CBR1) increases the levels of unsaturated fatty acids, which stimulate PM H^+-ATPase activity and thus lead to rhizosphere acidification. *CBR1*-overexpressing (*CBR1*-OX) *Arabidopsis thaliana* plants had higher levels of unsaturated fatty acids (18:2 and 18:3), higher PM H^+-ATPase activity, and lower rhizosphere pH than wild-type plants. By contrast, *cbr1* loss-of-function mutant plants showed lower levels of unsaturated fatty acids and lower PM H^+-ATPase activity but higher rhizosphere pH. Reduced PM H^+-ATPase activity in *cbr1* could be restored *in vitro* by addition of unsaturated fatty acids. Transcript levels of *CBR1*, *fatty acids desaturase 2* (*FAD2*), and *fatty acids desaturase 3* (*FAD3*) were increased under Fe-deficient conditions. We propose that CBR1 has a crucial role in increasing the levels of unsaturated fatty acids, which activate the PM H^+-ATPase and thus reduce rhizosphere pH. This reaction cascade ultimately promotes root Fe uptake.

Key words: cytochrome *b*5 reductase 1 (CBR1), unsaturated fatty acids, iron (Fe) uptake, H^+-ATPase

Oh Y.J., Kim H., Seo S.H., Hwang B.G., Chang Y.S., Lee J., Lee D.W., Sohn E.J., Lee S.J., Lee Y., and Hwang I. (2016). Cytochrome *b*5 Reductase 1 Triggers Serial Reactions that Lead to Iron Uptake in Plants. Mol. Plant. **9**, 501–513.

INTRODUCTION

Iron (Fe) is an essential element in all living organisms including plants (Bocca et al., 1984; Hänsch and Mendel, 2009; Lee et al., 2012), although excess Fe is toxic to cells. The optimum cellular Fe levels vary depending on plant growth, developmental stage, and environmental conditions (Clemens, 2001; Pilon et al., 2009; Walker and Waters, 2011). Thus, the mechanisms regulating Fe homeostasis must involve tight control of Fe uptake, utilization, storage, and translocation.

Different plant species use different strategies for soil Fe uptake. Non-graminaceous plants such as *Arabidopsis* use a three-step process to acquire Fe from soil, which is designated strategy I. The first step in strategy I is rhizosphere acidification via H^+ secretion to solubilize soil-bound Fe. This step is mediated by plasma membrane (PM)-localized H^+-ATPases. In the second step, ferric reductase oxidases (FROs) at the apoplast reduce Fe(III) to Fe(II); this step also is crucial for Fe uptake (Yi and Guerinot, 1996). The third step is performed by Fe transporters such as IRT1, which import Fe(II) into cells (Eide et al., 1996; Vert et al., 2002). The expression of genes encoding these Fe uptake-related proteins are induced under Fe-deficient conditions (Colangelo and Guerinot, 2004). Graminaceous plants such as rice and wheat release Fe-chelating molecules (phytosiderophores) that have high binding affinity for Fe(III). Phytosiderophore–Fe(III) complexes are imported into root cells by the yellow stripe/yellow stripe-like (YSL) transporter family.

Published by the Molecular Plant Shanghai Editorial Office in association with Cell Press, an imprint of Elsevier Inc., on behalf of CSPB and IPPE, SIBS, CAS.

Many factors contribute to Fe uptake from soil, one of which is rhizosphere acidification. A reduction of one pH unit leads to a 1000-fold increase in soil Fe solubility (Santi and Schmidt, 2009). PM H^+-ATPase activity is regulated at multiple levels under Fe-deficient conditions. *Arabidopsis AHA* genes encoding PM H^+-ATPases, particularly *AHA2* and *AHA7*, are expressed at higher levels under Fe-deficient conditions (Santi, and Schmidt, 2009). PM H^+-ATPase activity also is regulated at the post-translational level by phosphorylation and 14-3-3 proteins (Jahn et al., 1997). Modulation of fatty acid length and degree of desaturation in membranes is reported to affect PM H^+-ATPase activity (Palmgren et al., 1990), but it is not clear whether this is a regulatory mechanism for soil Fe uptake in plants.

Cytochrome *b*5 reductase (CBR) mediates electron transfer from NADH to cytochrome *b*5. *Arabidopsis* contains two CBR isoforms, CBR1 and CBR2, which localize to the ER membrane and mitochondrial inner membrane, respectively (Heazlewood et al., 2004; Kumar et al., 2006; Wayne et al., 2013). CBR1 has a key role in fatty acid desaturation in the ER membrane by transferring electrons from NADH to the heme group of cytochrome *b*5. NADH is generated in the cytosol during glycolysis (Threntham, 1971). Cytochrome *b*5 then transfers the electrons to fatty acids desaturase 2 (FAD2) and fatty acids desaturase 3 (FAD3), which introduce double bonds into fatty acids. It has been reported that the *cbr1-2* mutant plants have reduced levels of unsaturated fatty acids (particularly 18:3) in seeds (Kumar et al., 2006; Wayne et al., 2013), and that CBR1 has a crucial role in the normal functioning of male gametophytes (Wayne et al., 2013). Thus, CBR1 is a key factor in energy transfer to cellular processes that require energy. By contrast, mitochondrial CBR2 is involved in ATP production (Bernardi, and Azzone, 1981; Heazlewood et al., 2004).

In this study, we investigated the physiological role of *CBR1* using *cbr1-2* mutant and *CBR1*-overexpressing (*CBR1*-OX) *Arabidopsis* plants. Our study provides evidence that CBR1 has a crucial role in rhizosphere acidification via production of unsaturated fatty acids, which activate the PM H^+-ATPase. Rhizosphere acidification promotes soil Fe solubility. As a result, CBR1 contributes to the Fe uptake from soil.

RESULTS

CBR1 Expression Is Closely Correlated with Fe Accumulation in Seeds and Vegetative Tissues

To elucidate the physiological role of *CBR1* in plants, we examined the phenotypes of *Arabidopsis* plants overexpressing *CBR1* and its loss-of-function mutant, *cbr1-2*, in *Arabidopsis* (Wayne et al., 2013). Transgenic *CBR1*-OX plants were generated by introducing *CBR1* cDNA under the control of strong *Cauliflower mosaic virus* (CaMV) *35S* promoter. Two independent *CBR1*-OX lines with similar *CBR1* expression levels were selected for further analyses (Supplemental Figure 1). The *cbr1-2* allele carries a T-DNA insertion in the third exon of *CBR1* (Supplemental Figure 2) (Kumar et al., 2006; Wayne et al., 2013). The *CBR1*-OX and *cbr1-2* plants did not exhibit any gross morphological alterations. However, when we compared vegetative growth of wild-type (WT), *CBR1*-OX, and *cbr1-2* plants, differences in root growth, fresh weight, and seed size were observed (Figure 1A–1E). *CBR1*-OX and *cbr1-2* plants had longer and shorter roots, respectively, than WT plants. Similarly, *CBR1*-OX and *cbr1-2* plants had greater and reduced fresh weights, respectively, than WT plants. Seeds of *CBR1*-OX and *cbr1-2* plants were larger and smaller, respectively, than those of WT plants. These results indicate that CBR1 has a positive role in plant growth.

To elucidate the underlying cause of these phenotypic changes, we initially investigated the changes in seed size. We used transmission electron microscopy (TEM) to examine seed ultrastructure for WT, *cbr1-2*, and *CBR1*-OX plants. The seed TEM images reveal two major components in cotyledon cells, protein storage vacuoles (PSVs) and oil bodies (OBs) (Figure 2). There were noticeable differences in the OB numbers among the three plant types. OBs were sparsely packed with intervening empty spaces in *cbr1-2* mutant seeds (Figure 2A). To quantify the difference in OB numbers, we measured the levels of triacylglycerol (TAG), the main component of seed oils. TAG levels were 18.3% lower in *cbr1-2* mutant seeds, and 19.3% and 16.2% higher in *CBR1*-OX1 and *CBR1*-OX2 seeds, respectively, than the levels in WT seeds (Figure 2B). This result was consistent with the observed seed sizes for the three plant types.

The number of globoids in PSVs also differed among the three plant types. Globoids are crystals of phytic acid and mineral salts (including the elements Zn, Fe, Na, Mg, Mn, Al, and P), which serve as a source of minerals and phosphates during seed germination (Regvar et al., 2011). *CBR1*-OX seeds had more globoids than WT and *cbr1-2* seeds, whereas *cbr1-2* and WT seeds had essentially equivalent globoid numbers (Figure 2A and 2C). To quantify these differences at the biochemical level and elucidate the underlying molecular mechanisms, we measured Fe, Mn, Zn, and P levels in globoids using an inductively coupled plasma spectrometer. *CBR1*-OX1 and *CBR1*-OX2 seeds had 96.4% and 91% increases in Fe contents, respectively, compared with the levels in WT seeds (Figure 2D). By contrast, there were no significant differences in element contents in *cbr1-2* and WT seeds (Figure 2D). This result is consistent with the observation of equivalent globoid numbers in WT and mutant seeds. However, *CBR1*-OX1 and *CBR1*-OX2 seeds exhibited 26.2% and 24.8% reductions in Zn levels, respectively, compared with those of WT seeds, whereas *cbr1-2* and WT seeds had essentially equivalent Zn levels (Figure 2D). In plants, Fe and Zn accumulation patterns are inversely related (Shanmugam et al., 2011; Pineau et al., 2012), and Fe and Zn homeostasis is maintained through regulatory crosstalk (Sinclair and Kramer, 2012). For metal ions to be stored in globoids, positively charged ions must first be neutralized; phytic acid is involved in this process. The phosphorus content was 45.2% and 34.1% higher in *CBR1*-OX1 and *CBR1*-OX2 seeds, respectively, than in WT seeds (Figure 2D). There were no significant differences in seed Mn levels among the three plant types. These results suggest that CBR1 is involved in Fe accumulation in seed globoids.

We measured the Fe contents in shoot and root tissues of young, actively growing plants, and compared them with Mn and Zn

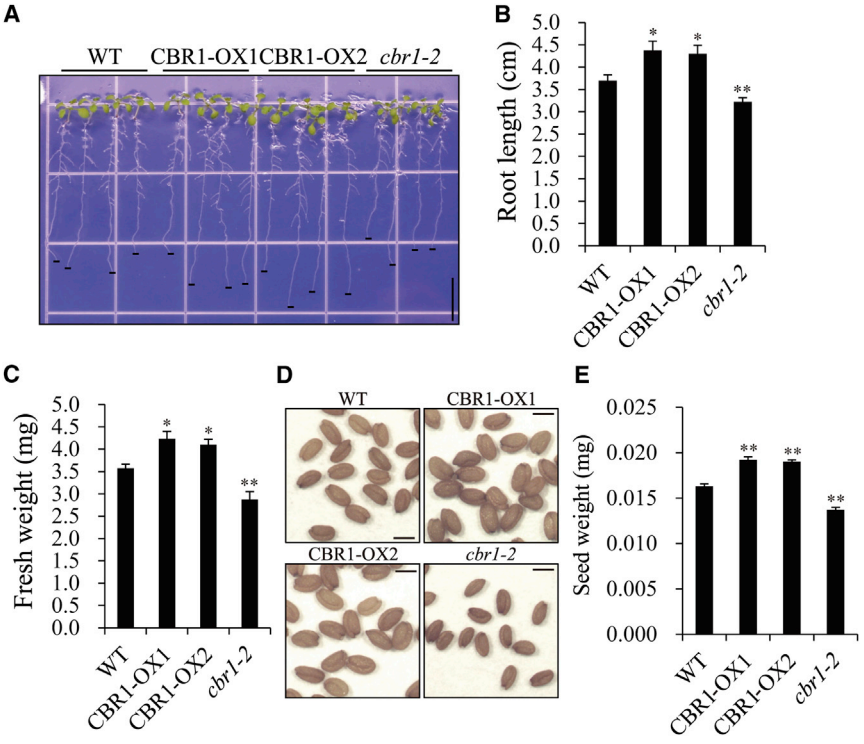

Figure 1. *CBR1* Expression Affects Plant Growth and Seed Morphology.

(A) Phenotype of *CBR1*-OX and *cbr1-2* mutant plants. Plants were grown on 1/2 MS medium for 14 days. Scale bar, 1 cm.

(B) Root length of *CBR1*-OX and *cbr1-2* mutant plants. Root length was measured 14 days after planting. Data represent mean ± SE (n = 45). P value was determined by Student's t-test. Asterisks indicate statistically significant differences ($^*P \leq 0.05$, $^{**}P \leq 0.01$) between WT and *CBR1*-OX1 or *CBR1*-OX2 plants, or between WT and *cbr1-2* plants.

(C) Fresh weight of *CBR1*-OX and *cbr1-2* mutant plants. Fresh weight was measured 14 days after planting. Data represent mean ± SE (n = 45). P value was determined by Student's t-test. Asterisks indicate statistically significant differences ($^*P \leq 0.05$, $^{**}P \leq 0.01$) between WT and *CBR1*-OX1 or *CBR1*-OX2 plants, or between WT and *cbr1-2* plants.

(D) Seed morphology. Scale bar, 0.5 mm.

(E) Seed weight measurement. Seed weight was measured using 500 seeds. Data represent mean ± SE (n = 3). P value was determined by Student's t-test. Asterisks indicate statistically significant differences ($^{**}P \leq 0.01$) between WT and *CBR1*-OX1 or *CBR1*-OX2 seeds, or between WT and *cbr1-2* seeds.

contents. Fe contents in *CBR1*-OX1 shoots and roots were 41.6% and 45.9% higher, respectively, than those in WT plants. Fe contents in *CBR1*-OX2 shoots and roots were 38.1% and 40.8% higher, respectively, than those in WT plants. By contrast, Zn levels were 15% and 37.4% lower in *CBR1*-OX1 shoots and roots, respectively, and 15.6% and 30.1% lower in *CBR1*-OX2 shoots and roots, respectively, than the levels in WT (Figure 3A and 3B). The accumulation patterns in *cbr1-2* mutants were inversely related to those observed in *CBR1*-OX plants. Fe contents were 39.1% and 33.6% lower in shoots and roots, respectively (Figure 3A and 3B), whereas Zn levels were 13.5% and 56.6% higher in shoots and roots, respectively, than those in WT plants (Figure 3A and 3B).

CBR1 Has a Role in Plant Responses to Extracellular Fe Concentrations

We investigated whether *CBR1* is involved in plant Fe uptake by examining root growth in WT, *CBR1*-OX, and *cbr1-2* plants on media containing different Fe concentrations (normal, Fe-deficient, and Fe-sufficient). Root length of all three types of plants was retarded under Fe-deficient conditions (300 μM Ferrozine) and enhanced under Fe-sufficient conditions (50 μM Fe), in agreement with a previous report (Giehl et al., 2012). Moreover, there were no significant differences in root lengths of the three plant types under both Fe-deficient and Fe-sufficient conditions, which contrasted with the root lengths of these three plant types on normal medium (1/2 Murashige and Skoog [MS]) (Figure 4A and 4B). These results indicate that the differential root growth observed depending on the expression *CBR1* can be overcome by Fe-sufficient conditions, and CBR1-mediated promotion of root growth can be inhibited under Fe-deficient conditions. To further clarify the relationships among medium Fe levels, *CBR1* expression, and plant growth, we examined how the three plant types responded to excess Fe (200 μM). Under excess extracellular Fe conditions, the three plant types all displayed severe growth retardation (Figure 4A and 4B). This result is consistent with the fact that excess Fe is detrimental to plant growth (Giehl et al., 2012). However, the plants differed in the degree of sensitivity to excess Fe. *CBR1*-OX and *cbr1-2* plants exhibited the highest and lowest sensitivity, respectively, to excess extracellular Fe (Figure 4A and 4B). Together, these results suggest that CBR1 is involved in Fe uptake.

To corroborate this result, we examined leaf chlorosis in WT, *cbr1-2*, and *CBR1*-OX plants under Fe-deficient conditions. Leaf chlorosis is a symptom of Fe deficiency (Vert et al., 2002; Lanquar et al., 2005). After short-term exposure to Fe-deficient conditions (300 μM Ferrozine), *cbr1-2* mutant plants exhibited a strong chlorotic phenotype, whereas *CBR1*-OX plants were not significantly affected and WT plants were only slightly affected (Figure 4C and 4D). This suggests that *CBR1* overexpression enhances Fe uptake under Fe-deficient conditions. The chlorotic phenotypes were rescued when plants were transferred to medium containing 50 μM $FeSO_4$ (Figure 4C and 4D). We also measured plant chlorophyll contents under normal (1/2 MS), Fe-deficient (300 μM Ferrozine), and Fe-rescue (50 μM $FeSO_4$) conditions. Under Fe-deficient conditions, the chlorophyll contents of *CBR1*-OX1 and *cbr1-2* mutant plants were 32.3% higher and 32.4% lower, respectively, than those of WT plants (Figure 4D). These results strongly support the hypothesis that CBR1 has an important role in Fe uptake in plants.

Overexpression of *CBR1* Upregulates PM H^+-ATPase Activity

We investigated how CBR1 contributes to soil Fe uptake. One possibility is that CBR1 is indirectly involved in Fe uptake

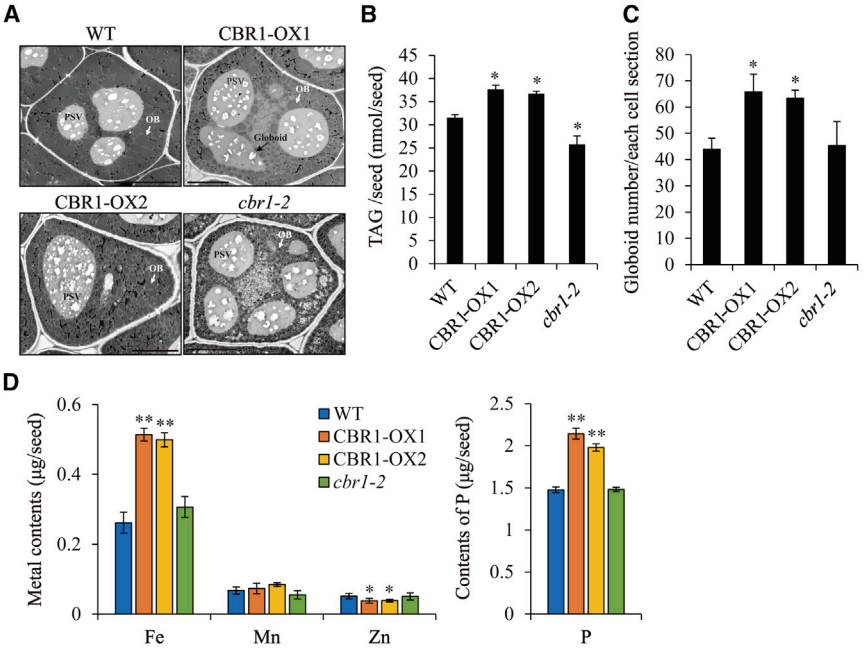

Figure 2. *CBR1* Overexpression Leads to Accumulation of Triacylglycerol and Fe in Seeds.

(A) Transmission electron microscopy images of ultrathin seed sections. PSV, protein storage vacuole; OB, oil body. Scale bar, 5 μm.

(B) TAG contents. Seeds were harvested from WT, *CBR1*-OX1, *CBR1*-OX2, and *cbr1-2* plants at the same time. TAG contents were measured using 500 seeds. Data are mean ± SE (n = 4). P value was determined by Student's t-test. Asterisks indicate statistically significant differences (*$P \leq 0.05$) between WT and *CBR1*-OX1 or *CBR1*-OX2 seeds, or between WT and *cbr1-2* seeds.

(C) Quantification of globoid numbers. The globoid number was counted on 20 sections. Five independent counts were performed. Data are mean ± SE (n = 100). P value was determined by Student's t-test. Asterisks indicate statistically significant differences (*$P \leq 0.05$) between WT and *CBR1*-OX1 or *CBR1*-OX2 seeds, or between WT and *cbr1-2* seeds.

(D) Element contents in seeds. Fe, Mn, Zn, and P amounts in 100 seeds were measured by inductively coupled plasma spectrometry. Data are mean ± SE (n = 6). P value was determined by Student's t-test. Asterisks indicate statistically significant differences (*$P \leq 0.05$, **$P \leq 0.01$) between WT and *CBR1*-OX1 or *CBR1*-OX2 seeds, or between WT and *cbr1-2* seeds.

because it is localized in the ER (Kumar et al., 2006; Wayne et al., 2013). We focused the investigation on rhizosphere acidification, and tested the rhizosphere pH surrounding the roots of the three plant types. Plants grown on normal medium (1/2 MS) for 14 days were transferred to 1/2 MS supplemented with 0.005% bromocresol purple (a pH indicator), and the color around the root tissues was examined 4 days after transfer. The rhizosphere pH was lower for *CBR1*-OX plants and higher for *cbr1-2* plants than that for WT plants, indicating that CBR1 is involved in rhizosphere acidification (Figure 5A). These results suggest that CBR1-mediated rhizosphere acidification may affect differential iron uptake among these plants.

To confirm this result *in planta*, we tested plant growth in alkaline soil (high pH). Soil pH was increased to 8–9 using calcium carbonate. Under these conditions, *CBR1*-OX plants displayed essentially normal growth, whereas *cbr1-2* plants displayed severely retarded growth (Supplemental Figure 3). This result suggests that *CBR1*-OX and *cbr1-2* plants have lower and higher rhizosphere pH, respectively, than that of WT plants.

We next examined how CBR1 contributes to rhizosphere acidification. The PM H^+-ATPase is responsible for rhizosphere acidification in plants, and PM H^+-ATPase activity closely correlates with plant Fe uptake (Sze et al., 1999; Santi and Schmidt, 2009). We prepared inside-out vesicles from PM fractions of WT, *CBR1*-OX1, *CBR1*-OX2, *cbr1-2*, and *cbr2-4* plants, and measured their ATPase activity (Figure 5B). The *cbr2-4* mutant is included as a control; CBR2 localizes to mitochondria and is involved in ATP production (Bernardi, and Azzone, 1981; Heazlewood et al., 2004). Vesicles from *CBR1*-OX plants had the highest sodium vanadate-sensitive ATPase activity, followed by vesicles from WT and *cbr1-2* plants. Vanadate-sensitive ATPase activity in *cbr2-4* vesicles was equivalent to that in WT. This indicates that CBR1 is involved in PM ATPase activation.

To determine whether the ATPase activity in the vesicles represents PM H^+-ATPase activity, we measured net H^+ efflux into the apoplast. Plants were grown on 1/2 MS plates for 10 days, then transferred to 1/2 MS liquid medium at pH 5.8 or pH 7.5 containing bromocresol purple with no buffering chemicals. We estimated the H^+ extrusion levels based on the medium color 24 h after transfer. At pH 5.8, WT, *cbr1-2*, and *cbr2-4* imported H^+ from the medium, with slightly higher import in *cbr1-2* than in WT or *cbr2-4* plants (Figure 5C). By contrast, *CBR1*-OX plants secreted H^+ into the medium at pH 5.8 (Figure 5C). At pH 7.5, all plants secreted H^+ into the medium; *CBR1*-OX plants had the highest H^+ secretion, followed by WT, *cbr2-4*, and *cbr1-2* plants (Figure 5C), indicating that CBR1 has a role in H^+ efflux across the PM. These combined results suggest that the higher PM ATPase activity measured in vesicles represents higher levels of H^+-ATPase activity.

We investigated how CBR1 activates PM H^+-ATPases. CBR1 localizes to the ER and functions in electron transfer from NADH to cytochrome *b5* (Percy and Lappin, 2008). NADH is generated primarily via glycolysis in the cytosol (Threntham, 1971). Thus, CBR1 may be indirectly involved in PM H^+-ATPase activation by regulating cellular ATP levels. We tested this hypothesis by determining cellular ATP levels. The ATP level was slightly higher in *CBR1*-OX plants and lower in *cbr1-2* plant than that in WT plants, but in both cases with no statistical significance (Figure 5D). The ATP level in *cbr2-4* mutant plants was 80% of that in WT, and was lower than that of *cbr1-2* mutant plants (Figure 5D). However, *cbr2-4* plants showed similar levels of ATPase activity and H^+-extrusion activity (compare Figure 5B and 5C). These results do not support the possibility that the

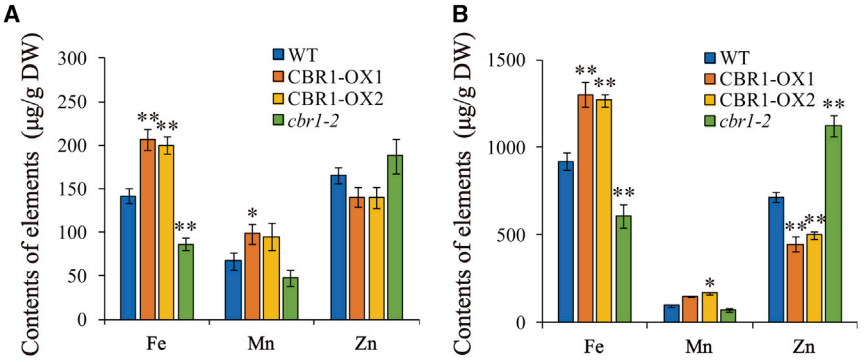

Figure 3. *CBR1* Expression Closely Correlates with Fe Accumulation in Plant Vegetative Tissues.

(A and B) Element contents in vegetative tissues. Amounts of indicated elements were measured using 0.1 g of shoots **(A)** or 0.01 g of roots **(B)** of 10-day-old plants. DW, dry weight. Data represent mean ± SE (n = 3). P value was determined by Student's t-test. Asterisks indicate statistically significant differences (*$P \leq 0.05$, **$P \leq 0.01$) between WT and *CBR1*-OX1 or *CBR1*-OX2 plants, or between WT and *cbr1-2* plants.

slightly different ATP levels in *cbr1-2* plants result in the observed differences in apoplastic pH.

We considered two other possible mechanisms for CBR1-mediated PM H^+-ATPase activation: (1) CBR1 increases *AHA* gene expression (*AHA* genes encode PM H^+-ATPases), and (2) CBR1 stimulates PM H^+-ATPase activity. In either case, CBR1 may indirectly promote PM H^+-ATPase activity. First, we examined *AHA2* and *AHA7* gene expression in WT, *CBR1*-OX1, and *cbr1-2* plants. These two *AHA* genes are induced under Fe-deficient conditions (Santi, and Schmidt, 2009). There were no significant differences in *AHA2* and *AHA7* expression levels in *CBR1*-OX1 plants, and the expression levels were only slightly higher than those in WT plants (Figure 5E). By contrast, *AHA2* and *AHA7* expression was strongly induced in *cbr1-2* mutant plants (Figure 5E). This result is in contrast to the lower levels of PM H^+-ATPase activity observed in *cbr1-2* (Figure 5B). To confirm the observed increase in *AHA* gene expression in *cbr1-2* plants, we prepared total protein extracts from WT, *CBR1*-OX1, and *cbr1-2* plants and subjected them to western blot analysis using an anti-H^+-ATPase antibody (anti-AHA antibody). Western blots confirmed that PM H^+-ATPase levels were higher in *cbr1-2* than in WT or *CBR1*-OX1 plants, indicating that *AHA* genes were expressed at higher levels in *cbr1-2* plants (Figure 5F and 5G). Thus, the protein levels (Figure 5F and 5G) did not correlate with the PM H^+-ATPase activity levels in the three plant types (Figure 5B). Specifically, higher PM H^+-ATPase protein levels in *cbr1-2* did not lead to higher PM H^+-ATPase activity levels. To understand this discrepancy in *cbr1-2* plants, we examined whether PM H^+-ATPase proteins are properly targeted to the PM. We isolated PM fractions from the total protein extracts of WT, *CBR1*-OX1, and *cbr1-2* and subjected them to western blot analysis using the anti-AHA antibody. Analysis of the PM fractions indicated that the *cbr1-2* PM fraction contained higher PM H^+-ATPase levels than those in WT or *CBR1*-OX1 extracts, indicating that H^+-ATPase is properly targeted to the PM in *cbr1-2* (Figure 5F and 5G). As controls for protein fractionation, we examined the PM protein PIP2 and the ER protein CRT1 using anti-PIP2 and anti-CRT1 antibodies, respectively. PIP2 but not CRT1 was detected in the PM fraction, confirming proper PM fractionation. These combined results indicate that *cbr1-2* plants do not have a defect in trafficking H^+-ATPase to the PM, but suggest that *cbr1-2* plants do have a defect in H^+-ATPase activation. It is possible that defective H^+-ATPase activation in *cbr1-2* plants leads to compensatory induction of *AHA2* and *AHA7* gene expression.

To further examine the effects of *cbr1-2* loss-of-function mutation and *CBR1* overexpression on *AHA* gene expression, we monitored *AHA2* and *AHA7* transcript levels at different growth stages. In *cbr1-2* plants, *AHA2* and *AHA7* expression continuously increased with age, with 4.3- and 4-fold induction, respectively, in 3-week-old plants. *AHA7* expression was continuously increased with age in both *CBR1-OX* and *cbr1-2* mutant plants, but at a lower level in *CBR1*-OX than in *cbr1-2* plants, whereas *AHA2* expression in *CBR1*-OX plants was slightly increased at 14 days after planting. In WT plants, both *AHA2* and *AHA7* expression was constant throughout the 3-week growth period (Supplemental Figure 4A and 4B). Next, we examined H^+-extrusion activity at different time points during the 3-week growth period. The H^+-extrusion activity of *cbr1-2* mutants was lower than that of WT plants at 6 days after planting, gradually increased with time, and reached WT levels at 21 days after planting (Supplemental Figure 4C). By contrast, the H^+-extrusion activity in *CBR1*-OX plants was higher than that in WT plants throughout the 3-week growth period. Thus, extracellular medium pH was more acidic with *CBR1*-OX plants than with WT plants. In *cbr1-2* mutant plants, the PM H^+-ATPase activity level (inferred by the medium pH) gradually recovered to WT levels during the 3-week growth period. This is likely due to a gradual increase in *AHA* gene expression with time. Moreover, at a later stage of plant growth, Fe levels in *cbr1-2* mutant plants also recovered to WT levels, confirming the correlation between the pH and Fe levels (Supplemental Figure 4D).

CBR1-Mediated Increase in Unsaturated Fatty Acids Activates PM H^+-ATPase

We examined the mechanism by which CBR1 activates PM H^+-ATPase. CBR1 is involved in desaturation of fatty acids (Kumar et al., 2006; Wayne et al., 2013). Therefore, we hypothesized that ER-localized CBR1 modulates the levels of unsaturated fatty acids in the ER membrane, which subsequently results in changes in the levels of unsaturated fatty acids in the PM, which affect PM H^+-ATPase activity. Unsaturated fatty acids generated in the ER can be transported to the PM by vesicle trafficking (Kaplan and Simoni, 1985). In support of this hypothesis, previous studies showed that unsaturated fatty acids activate H^+-ATPase *in vitro* (Palmgren et al., 1988, 1990). We examined lipids in WT, *CBR1*-OX1, and *cbr1-2* plants. Previous work showed that *cbr1-2* mutant plants exhibited significantly reduced levels of unsaturated fatty acids in triacylglycerides, particularly linolenic acid (C18:3), in seeds; however, no

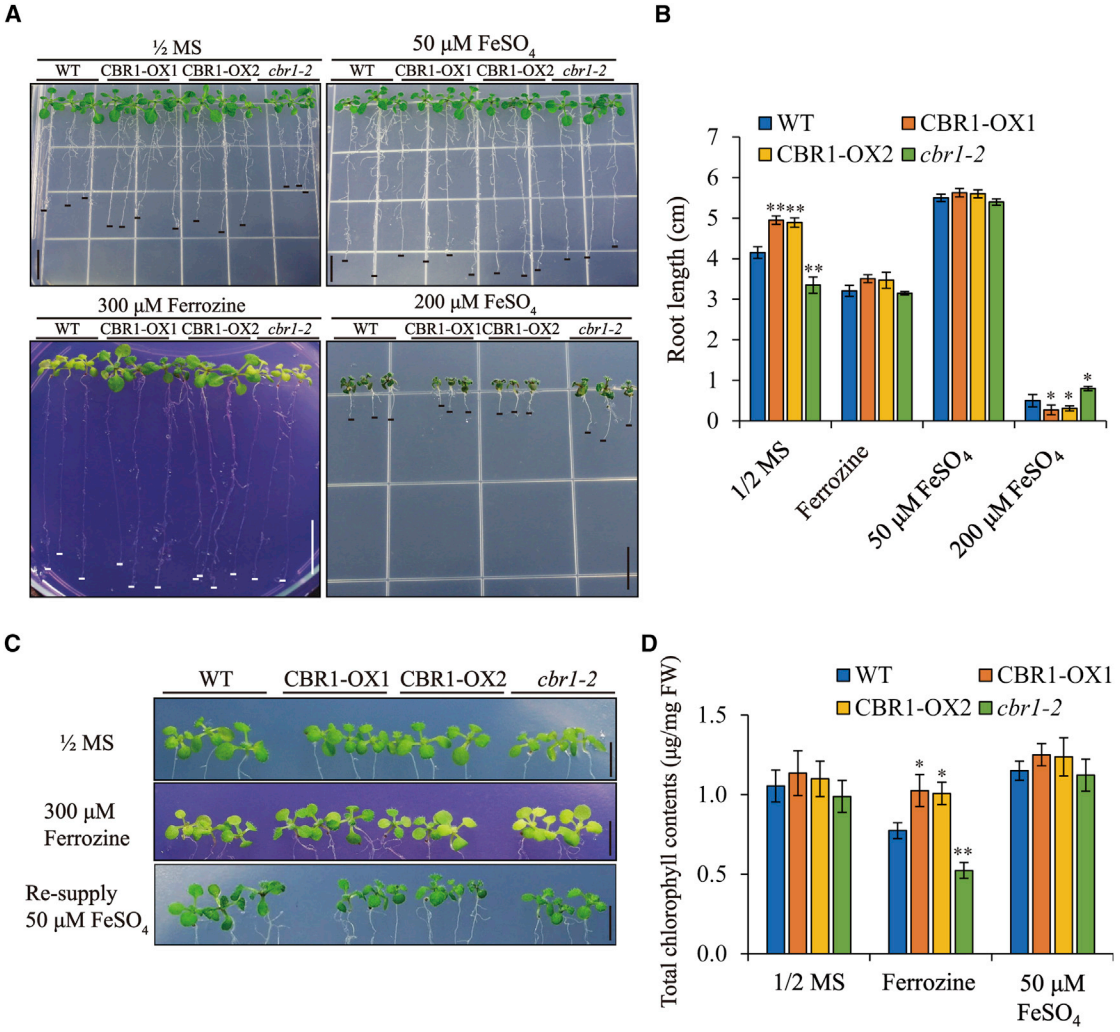

Figure 4. *CBR1* Expression Affects Plant Responses to External Fe Conditions.

(A and B) Effect of *CBR1* expression on plant responses to Fe-excess or Fe-deficient conditions. **(A)** Plants were grown on 1/2 MS plates supplemented with 1.0% sucrose with or without the indicated $FeSO_4$ concentrations. To measure the Fe-deficiency effect, plants grown on 1/2 MS plates for 7 days were transferred to 1/2 MS plates supplemented with 300 μM Ferrozine and grown for an additional 7 days. Scale bar, 1 cm. **(B)** To quantify the effect of external Fe conditions on root growth, we measured the root length 15 days after planting. Data represent mean ± SE ($n = 45$). *P* value was determined by Student's *t*-test. Asterisks indicate statistically significant differences (*$P \leq 0.05$, **$P \leq 0.01$) between WT and *CBR1*-OX1 or *CBR1*-OX2 plants, or between WT and *cbr1-2* plants.

(C) Leaf chlorosis under Fe-deficient conditions. Plants grown on 1/2 MS plates for 7 days (top panel) were transferred to 1/2 MS plates supplemented with 300 μM Ferrozine and grown for an additional 5 days (middle panel). Subsequently, plants shown in the middle panel were transferred again to 1/2 MS plates supplemented with 50 μM $FeSO_4$ and grown for 5 days. Scale bar, 1 cm.

(D) Measurement of chlorophyll contents. Plants grown on 1/2 MS for 7 days were transferred to 1/2 MS supplemented with 300 μM Ferrozine. Chlorophyll contents were measured 4 days after transfer. FW, fresh weight. Data represent mean ± SE ($n = 45$). *P* value was determined by Student's *t*-test. Asterisks indicate statistically significant differences (*$P \leq 0.05$, **$P \leq 0.01$) between WT and *CBR1*-OX1 or *CBR1*-OX2 plants, or between WT and *cbr1-2* plants.

significant differences for the levels of unsaturated fatty acids in vegetative tissues were observed (Kumar et al., 2006; Wayne et al., 2013). We examined the lipid composition in root tissues of young seedlings. The three plant types exhibited differences in lipid composition. In *cbr1-2* plants, the levels of the saturated fatty acids palmitic acid (16:0) and stearic acid (18:0) increased by 23.5% and 40% (in molar %), respectively, whereas the levels of the unsaturated fatty acids oleic acid (18:1), linoleic acid (18:2), and linolenic acid (18:3) decreased by 24.8%, 22.9%, and 24.2%, respectively, compared with those in WT plants (Figure 6A). By contrast, *CBR1*-OX1 roots had reductions in the levels of the saturated fatty acids palmitic acid (16:0), stearic acid (18:0), and oleic acid (18:1) by 4.6%, 16.2%, and 21.6%, respectively, and increases in the levels of the unsaturated fatty acids linoleic acid (18:2) and linolenic acid (18:3) by 12% and 16.1%, respectively, compared with those in WT plants (Figure 6A). These results indicate that CBR1 increases the levels of unsaturated fatty acids in root tissues. To confirm these results independently, we tested these three plant types for freezing stress tolerance and response. Plants

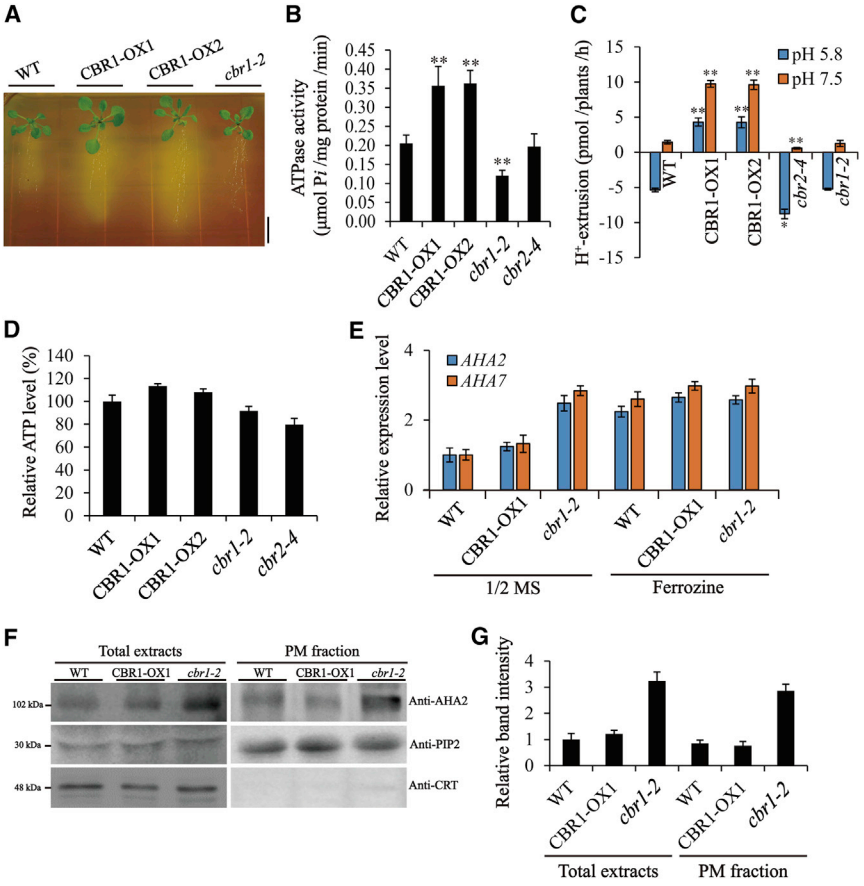

Figure 5. *CBR1* Has a Role in PM H$^+$-ATPase Activation and H$^+$ Extrusion into the Rhizosphere.

(A) Visualization of rhizosphere acidification. Plants grown on 1/2 MS medium for 10 days were transferred to 1/2 MS (pH 6.5), supplemented with 0.005% bromocresol purple as pH indicator. Image was taken 4 days after transfer. Scale bar, 1 cm. The pH indicator shows a yellow color at acidic pH and a purple color at alkaline pH.

(B) Vanadate-sensitive PM ATPase activity. Inside-out vesicles were used to measure PM ATPase activity. ATPase activity indicates the amount of P_i released from ATP hydrolysis for 10 min. A_{850} values were used to calculate P_i amounts using the standard curve shown in Supplemental Figure 7A. Data represent mean ± SE (n = 4). P value was determined by Student's t-test. Asterisks indicate statistically significant differences (**$P \leq 0.01$) between WT and *CBR1*-OX1 or *CBR1*-OX2 plants, between WT and *cbr1-2* plants, and between WT and *cbr2-4* plants.

(C) Proton efflux activity. Plants grown on 1/2 MS plates for 10 days were transferred to 1/2 MS liquid medium at pH 5.8 or pH 7.5 without MES but containing bromocresol purple (0.005%). A_{580} was measured 24 h after transfer. H$^+$ concentration was calculated using the standard curve shown in Supplemental Figure 7B. Data represent mean ± SE (n = 4). P value was determined by Student's t-test. Asterisks indicate statistically significant differences (**$P \leq 0.01$) in pH values between WT and *CBR1*-OX1 or *CBR1*-OX2 plants, between WT plants and *cbr1-2* plants, or between WT and *cbr2-4* plants.

(D) Quantification of ATP levels in root tissues. Relative ATP level was measured in 7-day-old plants.

(E) *AHA2* and *AHA7* transcript levels under normal and Fe-deficient conditions. Total RNA from root tissues of WT, *CBR1*-OX1, and *cbr1-2* plants was used to examine the indicated *AHA* transcript levels by qRT–PCR. *Actin 2* was used as an internal control. Plants were vertically grown on 1/2 MS plates for 10 days, and transferred to 1/2 MS medium or 1/2 MS supplemented with 300 μM Ferrozine. Total RNA was isolated 2 days after transfer. Data represent mean ± SE (n = 3).

(F and G) PM H$^+$-ATPase levels. **(F)** PM fractions were prepared from total protein extracts by ultracentrifugation, and were subjected to western blot analysis using anti-H$^+$-ATPase, anti-PIP2, and anti-CRT antibodies. PIP2 and CRT were used as markers of PM and ER membrane proteins, respectively. **(G)** To quantify AHA levels, band intensity was measured using imaging software. Total extracts, unfractionated total protein extracts; PM fraction, plasma membrane fraction.

enhance their freezing tolerance by increasing the levels of unsaturated fatty acids (Kodama et al., 1994; Chen and Thelen, 2013). The results showed that *CBR1*-OX plants exhibited enhanced freezing tolerance, whereas *cbr1-2* plants exhibited increased sensitivity to freezing stress compared with that in WT plants (Supplemental Figure 5). These results confirm that *CBR1*-OX and *cbr1-2* plants have higher and lower levels of unsaturated fatty acids, respectively, than that of WT plants (Supplemental Figure 5).

Next, we confirmed that *Arabidopsis* PM ATPase is activated by unsaturated fatty acids *in vitro*, as reported previously (Palmgren et al., 1988, 1990). We prepared PM vesicles from WT plants, supplemented with one of three different types of fatty acids (18:0, 18:2, or 18:3) at three different concentrations (20, 50, and 100 μM), and measured ATPase activity. Consistent with previous results (Palmgren et al., 1988, 1990), supplementation with 20 or 50 μM of the unsaturated fatty acids linoleic acid (18:2) or linolenic acid (18:3) strongly activated ATPase, with less activation at 100 μM, whereas stearic acid supplementation only slightly activated ATPase or did not activate it, depending on the concentration (Figure 6B). These results support the hypothesis that CBR1-mediated increases in the levels of unsaturated fatty acids *in planta* lead to H$^+$-ATPase activation, which, in turn, results in enhanced H$^+$ extrusion into the rhizosphere.

To corroborate this result, we examined H$^+$-ATPase activity in the fatty acid desaturase *fad2-1* and *fad3-2* loss-of-function mutant plants that were defective in production of 18:2 and 18:3, respectively (Figure 6C). We prepared PM microsomes and measured ATPase activity. Similarly to *cbr1-2*, *fad2-1* plants had lower ATPase activity than that of WT plants; *fad3-2* plants had slightly lower ATPase activity than that of WT plants, but this difference was not statistically significant. The 18:2 fatty acids accumulate to higher levels in *fad3-2* mutants (Browse et al., 1993), which may compensate for the loss of 18:3-mediated PM H$^+$-ATPase activation. These results prompted us to test whether 18:2 or 18:3 supplementation to *cbr1-2* PM microsomes can rescue H$^+$-ATPase activity (Figure 6D). The results showed

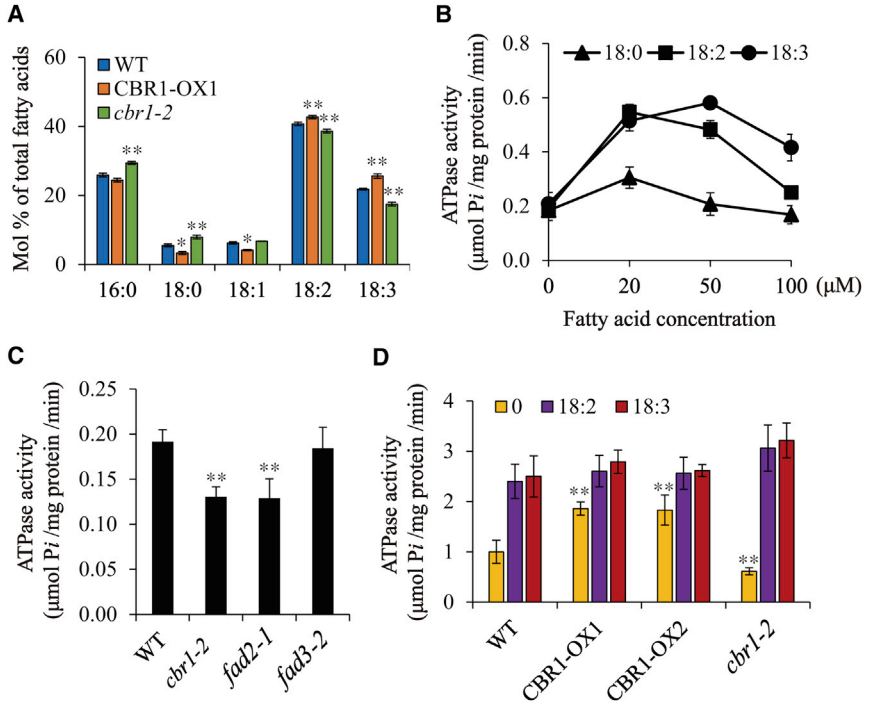

Figure 6. CBR1 Is Involved in Producing 18:2 and 18:3 Unsaturated Fatty Acids, which Activate PM H$^+$-ATPase *In Vitro*.

(A) CBR1 effect on fatty acid composition. Fatty acids were determined in root tissues of plants grown on 1/2 MS plates for 10 days. Values represent the relative molar percent. Data represent mean ± SE (n = 6). P value was determined by Student's t-test. Asterisks indicate statistically significant differences ($^*P \leq 0.01$, $^{**}P \leq 0.01$) between WT and *CBR1*-OX1 roots, or between WT and *cbr1-2* roots.

(B) Effect of unsaturated fatty acids on PM ATPase activity *in vitro*. PM vesicles of WT plants were supplemented with the indicated fatty acids at the indicated concentrations. ATPase activity was measured as described in Figure 5B.

(C) Comparison of vanadate-sensitive PM ATPase activities between *cbr1-2* and *fad2-1* or *fad3-2* plants. ATPase activity was measured as described in Figure 5B. Data represent mean ± SE (n = 4). P value was determined by Student's t-test. Asterisks indicate statistically significant differences ($^{**}P \leq 0.01$) between WT and *cbr1-2* roots, between WT and *fad2-1* roots, or between WT and *fad3-2* roots.

(D) Rescue of H$^+$-ATPase activity in *cbr1-2* mutant plants. PM vesicles of WT, *CBR1*-OX1, *CBR1*-OX2, and *cbr1-2* plants were supplemented with 20 μM 18:2 or 18:3 fatty acids. ATPase activity was measured as described in Figure 5B. Data represent mean ± SE (n = 4). P value was determined by Student's t-test. Asterisks indicate statistically significant differences ($^{**}P \leq 0.01$) between WT and *CBR1*-OX1 roots or between WT and *cbr1-2* roots.

that 18:2 or 18:3 supplementation greatly enhanced H$^+$-ATPase activity in PM microsomes of WT, *CBR1*-OX, and *cbr1-2* plants, with slightly higher H$^+$-ATPase activity in *cbr1-2* than in *CBR1*-OX or WT plants. The higher AHA2 protein levels in *cbr1-2* than in *CBR1*-OX or WT plants might have contributed to higher H$^+$-ATPase activity in *cbr1-2* plants than in *CBR1*-OX or WT plants (Figure 5F).

CBR1 Facilitates Fe Uptake via Rhizosphere Acidification

To test whether differences in Fe contents in the three plant types is directly related to differences in rhizosphere pH, we compared Fe contents in plants grown in pH 5.8 media with or without buffering capacity. Proton secretion into the root apoplast can induce a rhizosphere pH change when plants are grown in non-buffered medium, but not when grown in buffered medium. In *CBR1*-OX1 and *CBR1*-OX2 plants, Fe contents were reduced by 21.8% and 24.1% in buffered media, respectively, compared with those in non-buffered media. By contrast, Fe content in *cbr1-2* mutant plants was increased by 22.6% in buffered medium compared with that in non-buffered medium (Figure 7A), and the Fe content in *cbr1-2* was statistically lower than that of WT plants. These results indicate that *cbr1-2* plants import less Fe in non-buffered medium than in buffered medium at pH 5.8. This is consistent with the observation that, at pH 5.8, *cbr1-2* plants import protons from medium but do not secrete protons into the medium (Figure 5C).

To gain further insight into the role of CBR1 in Fe uptake and accumulation, we examined the expression of genes involved in Fe homeostasis. We compared the expression of genes encoding PM-localized transporter 1 (*IRT1*) and transcription factor 1 (*FIT1*) in WT, *CBR1*-OX1, and *cbr1-2* plants (Eide et al., 1996; Vert et al., 2002; Colangelo and Guerinot, 2004), as well as genes encoding a ferric chelate reductase (FRO2) (Robinson et al., 1999; Connolly et al., 2003) as representatives of Fe homeostasis-related genes. *IRT1*, *FRO2*, and *FIT1* were expressed at higher levels in *cbr1-2* plants than in WT plants (Supplemental Figure 6). Thus, the expression patterns of these genes were closely correlated with the cellular levels of Fe in *cbr1-2*. Interestingly, *IRT1* and *FIT1*, except *FRO2*, were also expressed at slightly higher levels in *CBR1*-OX1 plants (Supplemental Figure 6), suggesting that CBR1 have an effect on the Fe homeostasis-related gene expression.

Next, we tested the effect of *CBR1* expression on the activity of ferric chelate reductase, which is a key factor involved in Fe uptake. We measured the ferric chelate reductase activity in three types of plants. *cbr1-2* mutant plants showed higher levels of ferric reductase activity, whereas *CBR1*-OX plants did not display any significant difference, compared with WT plants (Figure 7B). These results are consistent with the expression levels of *FRO2*. However, linolenic acids (18:3) did not have any effect on the activity of ferric chelate reductase (Figure 7C), indicating that the higher activity of ferric chelate reductase in *cbr1-2* plants resulted predominantly from higher expression level of *FRO2* gene.

Unsaturated Fatty Acids, 18:2 and 18:3, Increase in Root Tissues under Fe-Deficient Conditions

To further examine the relationship between Fe uptake and *CBR1*, we examined the expression of *CBR1*, *FAD2*, and *FAD3*

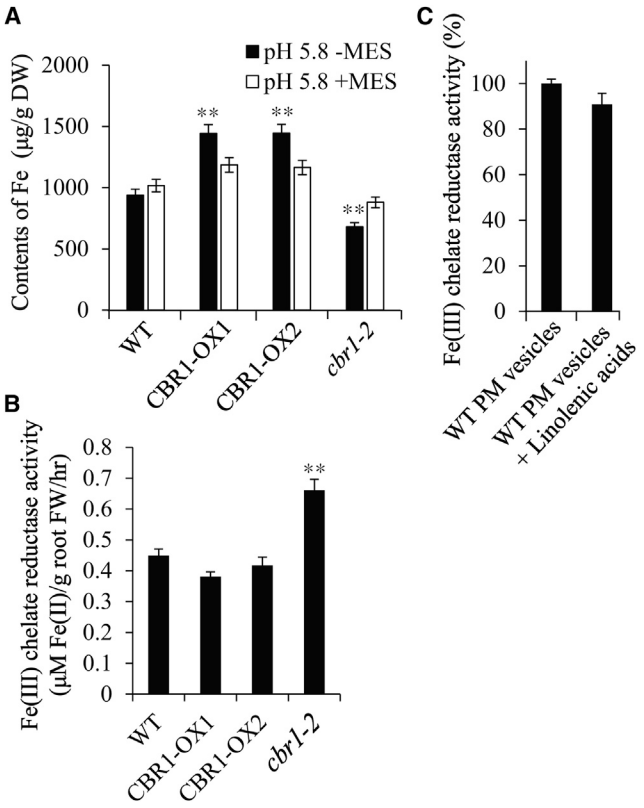

Figure 7. CBR1 Facilitates Fe Uptake via Rhizosphere Acidification.

(A) Fe contents in three types of plants depending on MES. Fe contents were measured in roots of plants grown for 10 days in 1/2 MS liquid media at pH 5.8 with or without 20 mM MES. Data represent mean ± SE (n = 4). P value was determined by Student's t-test. Asterisks indicate statistically significant differences (**$P \leq 0.01$) between WT and *CBR1*-OX1 or *CBR1*-OX2 plants, or between WT and *cbr1-2* plants, grown under the same conditions.

(B) Fe(III) chelate reductase activity. Plants grown on 1/2 MS plates for 2 weeks were incubated in 0.1 mM Fe(III)–EDTA and 0.3 mM Ferrozine solution for 90 min. The amount of purple-colored Fe(II)–Ferrozine complexes was measured by absorbance at 562 nm. P value was determined by Student's t-test. Asterisks indicate statistically significant differences (**$P \leq 0.01$) between WT and *CBR1*-OX1 or *CBR1*-OX2 plants, or between WT and *cbr1-2* plants.

(C) The effect of linolenic acids (18:3) on Fe(III) chelate reductase activity. The PM vesicles extracted from roots of 2-week-old WT plants were supplemented with 50 μM linolenic acids (18:3). Ferric chelate reductase activity was measured as described in Figure 7B.

under Fe-deficient conditions. We analyzed *AHA2* and *AHA7* expression as positive controls, because they are known to be induced under Fe-deficient conditions (Santi, and Schmidt, 2009). *CBR1*, *FAD2*, and *FAD3* expression patterns were induced similarly to those of *AHA2* and *AHA7* under Fe-deficient conditions, with gradual increases in expression levels up to 30 h after the start of Fe deficiency (Figure 8A). To corroborate induction of *CBR1* expression, we determined CBR1 protein levels by western blot analysis using anti-CBR1 antibody. CBR1 protein levels increased similarly with its transcript levels (Figure 8B). Next, we examined whether Fe-deficient conditions induce changes in the levels of unsaturated fatty acids. We determined fatty acid levels at specified times after the start of Fe-deficient conditions (Figure 8C). The composition of fatty acids did not show any significant changes up to 6 h after the start of Fe deficiency. However, the 18:3 unsaturated fatty acid increased substantially at 18 and 30 h, and 18:2 increased significantly at 30 h after the start of Fe deficiency. These results were consistent with the patterns of *CBR1*, *FAD2*, *FAD3*, and *AHA* gene expression. This indicates that plants increase the levels of 18:2 and 18:3 unsaturated fatty acids in response to the Fe-deficient conditions.

DISCUSSION

This study presents evidence that *CBR1* expression is closely correlated with Fe content in root tissues. A role for CBR1 in regulating plant Fe content was clearly demonstrated by the observation that *CBR1*-OX and *cbr1-2* plants had higher and lower Fe levels, and higher and lower sensitivity to excess Fe conditions, respectively. This relationship between CBR1 and Fe content was not recognized in previous studies. *Arabidopsis* contains two CBR isoforms, CBR1 and CBR2 (Kumar et al., 2006; Wayne et al., 2013). CBR1 transfers electrons from NADH to cytochrome *b*5 at the ER membrane (Kumar et al., 2006; Wayne et al., 2013), whereas CBR2 localizes to mitochondria and is involved in ATP production (Bernardi, and Azzone, 1981; Heazlewood et al., 2004). NADH is largely produced by glycolysis in the cytosol (Threntham, 1971). Therefore, CBR1 is in effect channeling cellular energy derived from glucose to various cellular processes. One important cellular process that uses the electron transferred by CBR1 from NADH is fatty acid desaturation by FAD2 and FAD3 at the ER membrane (Kumar et al., 2006; Wayne et al., 2013). Therefore, the CBR1-transferred electron serves to increase the levels of unsaturated fatty acids in cellular membranes. Consistent with this proposal, *cbr1-2* plants exhibited reduced levels of 18:3 unsaturated fatty acids in seeds. In this study, we provide evidence that CBR1 also has a role in production of 18:2 and 18:3 unsaturated fatty acids in vegetative tissues. This observation is based on our analysis of fatty acids in root tissues of young plants. Consistent with these biochemical data, *CBR1*-OX and *cbr1-2* plants display enhanced resistance and increased sensitivity to freezing, respectively (Supplemental Figure 5). The levels of unsaturated fatty acids in plants increase in response to low temperature or freezing conditions (Chen and Thelen, 2013). However, our result differs from that of a previous study, which reported that the fatty acid composition in vegetative tissues of *cbr1-2* plants did not differ from that of WT plants (Wayne et al., 2013). It is possible that this discrepancy in the two studies is due to differences in the plants examined; the current study used 10-day-old seedlings for the experiment, whereas the previous study used 20-day-old plants. Plant fatty acid composition is reported to depend on the growth stage (Miquel and Browse, 1992; Hernandez and Cooke, 1997; Lopez-Villalobos et al., 2001). The current study suggests that CBR1 has a key role in increasing the unsaturated fatty acid level in plant tissues under specific intrinsic or environmental conditions.

We examined rhizosphere acidification as the potential mechanism of CBR1-mediated plant Fe uptake. The effect of CBR1 on soil Fe uptake should occur indirectly because CBR1 localizes to the ER. One of the major routes of soil Fe uptake in *Arabidopsis* is transporter-mediated import of free Fe. This necessitates solubilization of Fe bound to the soil, which is enhanced under acidic

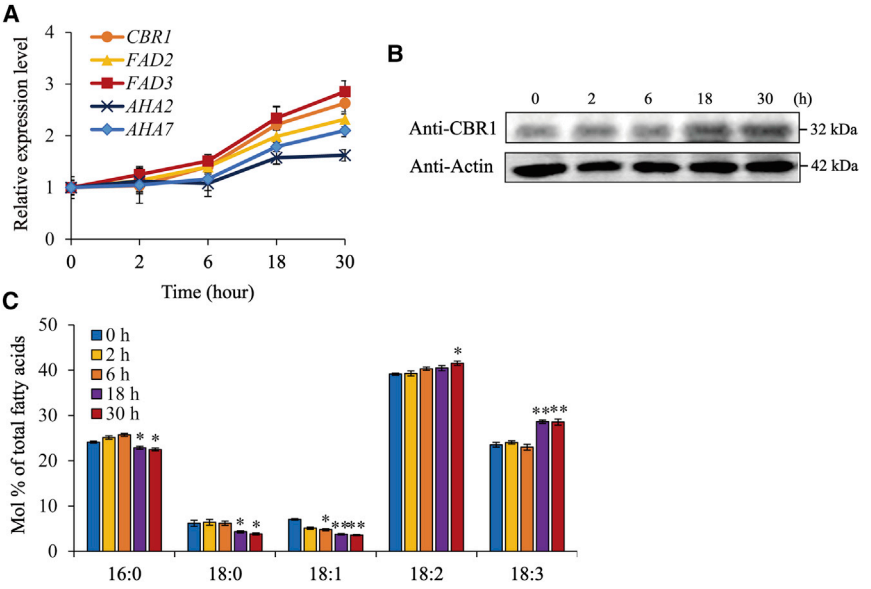

Figure 8. Fe-Deficient Conditions Induce *CBR1*, *FAD2*, and *FAD3* Expression, and Increase Unsaturated Fatty Acid Levels.

(A) *CBR1*, *FAD2*, *FAD3*, *AHA2*, and *AHA7* induction under Fe-deficient conditions. Plants were grown on 1/2 MS plates (pH 5.8), supplemented with 1% sucrose for 7 days, transferred to 1/2 MS plates (pH 5.8), supplemented with 1% sucrose plus 300 μM Ferrozine, and then grown for the indicated time periods. Total RNA was prepared and used for qRT–PCR analysis. *Actin2* was used as internal control. Data represent mean ± SE (n = 3).

(B) CBR1 levels under Fe-deficient conditions. Plants were grown as described in **(A)**. Protein extracts (10 μg) were separated by SDS–PAGE and subjected to western blot analysis using anti-CBR1 and anti-actin antibodies. Actin was used as loading control.

(C) Increase of the levels of unsaturated fatty acids in WT root tissues under Fe-deficient conditions. Plants were grown as described in **(A)**. Fatty acid composition was determined in roots. Values represent the relative molar percent. Data represent mean ± SE (n = 4). P value was determined by Student's t-test. Asterisks indicate statistically significant differences (*$P \leq 0.01$, **$P \leq 0.01$) between WT and *CBR1*-OX1 root tissues, or between WT and *cbr1-2* root tissues.

conditions. Thus, rhizosphere acidification is one of the key factors required for soil Fe uptake (Curie et al., 2000; Vert et al., 2002). A reduction of one pH unit increases Fe solubility by 1000-fold (Santi and Schmidt, 2009). In plants, PM H^+-ATPase has a major role in rhizosphere acidification by secreting H^+ into the apoplast (Sze et al., 1999; Santi and Schmidt, 2009). Thus, we hypothesized that CBR1 directly or indirectly affected rhizosphere pH. The results showed that *CBR1*-OX plants had a more acidic rhizosphere, whereas *cbr1-2* plants had a less acidic rhizosphere than that of WT.

Plant rhizosphere acidification can be regulated at multiple levels. We ruled out the possibility that reduced ATP levels or PM H^+-ATPase levels were the underlying cause of reduced Fe content in *cbr1-2* plants. We found that *cbr1-2* plants had higher PM H^+-ATPase levels, although they had lower PM ATPase activity. At present, the mechanism underlying enhanced *AHA2* and *AHA7* expression in *cbr1-2* plants is not clearly understood. The *cbr2-4* mutant plants had lower ATP levels than those of *cbr1-2* plants, but they did not significantly differ in PM ATPase activity. We hypothesized that PM H^+-ATPase activation has a key role in the relationship between CBR1 and Fe contents in plants. PM H^+-ATPase has an amphipathic structure, and its activity is regulated by the hydrophobic environment in the PM (Palmgren et al., 1988, 1990). This is different from the activation mediated by phosphorylation and 14-3-3 proteins (Jahn et al., 1997). H^+-ATPase activity is also affected by the lipid composition of the membrane to which H^+-ATPase localizes, and the acyl chain length and degree of fatty acid unsaturation (Palmgren et al., 1988, 1990). *CBR1*-OX and *cbr1-2* mutant plants had higher and lower levels of unsaturated fatty acids, higher and lower H^+-extrusion activity, and more acidic and less acidic rhizosphere, respectively. Consistent with these *in planta* results, the PM ATPase in *Arabidopsis* is activated by 18:2 and 18:3 unsaturated fatty acids *in vitro*, in agreement with the results of previous studies (Palmgren et al., 1988, 1990). Furthermore, supplementation of PM-derived microsomes of *cbr1-2* plants with 18:2 and 18:3 unsaturated fatty acids rescued ATPase activity to higher levels than those of WT and *CBR1*-OX. These combined results indicate that CBR1 has an important role in H^+-ATPase activation by increasing the levels of unsaturated fatty acids. FAD2 and FAD3 fatty acid desaturases have key roles in this process because CBR1 provides electrons to these enzymes from NADH via cytochrome *b*5 (Wayne et al., 2013). We conclude that *CBR1* expression stimulates production of the PM H^+-ATPases activators (18:2 and 18:3), which enhances PM H^+-ATPase activity and subsequently leads to rhizosphere acidification. Consistent with this hypothesis, *fad2* mutant plants also displayed lower PM ATPase activity, which was similar to that of *cbr1-2* plants. During Fe-deficient conditions, *CBR1*, *FAD2*, and *FAD3* expression was induced in WT plants, and 18:2 and 18:3 unsaturated fatty acids increased to higher levels. As reported previously (Santi and Schmidt, 2009) and confirmed by this study, the increase in PM H^+-ATPase levels is one of the mechanisms used to cope with lower Fe contents in plants under Fe-deficient conditions. Thus, plants employ two different strategies to induce rhizosphere acidification under Fe-deficient conditions: by increasing *AHA* gene expression and H^+-ATPase levels, and by activating H^+-ATPase via the process described in this study (Figure 9).

In summary, our study provides compelling evidence that CBR1 contributes to Fe uptake in plants. CBR1 functions as a trigger in a series of reactions consisting of electron transfer from NADH to cytochrome *b*5, fatty acid desaturation by FAD2 and FAD3, activation of PM H^+-ATPases, and rhizosphere acidification, which in turn facilitates root Fe uptake. This study indicates that CBR1 contributes to Fe uptake by channeling cellular energy to the essential cellular pathway mediating plant Fe uptake.

METHODS

Plant Growth Conditions

Arabidopsis thaliana (Colombia ecotype) plants were grown on 1/2 MS agar plates supplemented with 1% sucrose in a growth chamber at

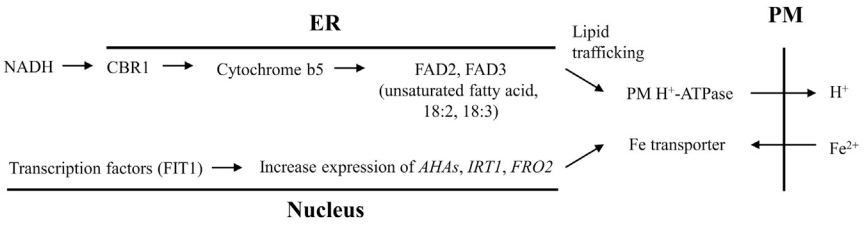

Figure 9. A Model for the Bifurcated Activation of Fe Uptake.

Fe uptake is enhanced via transcription factor (FIT1)-mediated increases in the expression of *IRT1*, *FRO2*, and *AHAs*. In addition, CBR1 plays a role in Fe uptake by transferring high-energy electrons from NADH to cytochrome *b*5, then to fatty acid desaturases, to produce unsaturated fatty acids 18:2 and 18:3, which function as activators of PM H^+-ATPase, thereby enhancing secretion of H^+ across the PM to acidify the rhizosphere. The acidic conditions in the rhizosphere enhance the solubility of Fe from the soil, thereby facilitating Fe uptake in plants.

22.5°C under a 16-h light/8-h dark cycle with relative humidity of 40%. To grow plants under Fe-deficient or Fe-excess conditions, Ferrozine (300 μM) or $FeSO_4$ (50 or 200 μM), respectively, were added to 1/2 MS medium containing 1% sucrose. To prepare soil at pH 8–9, the pH of the soil was adjusted with calcium carbonate. For liquid culture of plants, 50-ml aliquots of liquid 1/2 MS medium were prepared. The medium pH was adjusted with 1 N KOH. Medium buffering capacity was provided with 10 mM 2-(N-morpholino)ethanesulfonic acid (MES) (pH 5.8).

Plasmid DNA Construction

Full-length *CBR1* cDNA was obtained from an *Arabidopsis* cDNA library prepared from leaf tissue; *CBR1* was amplified by PCR using primers CBR1-5 and CBR1-3. To generate *CBR1:sGFP*, the PCR product was digested with restriction endonucleases *Xho*I and *Kpn*I, and inserted into pUC-GFP digested with *Xho*I and *Kpn*I downstream of the cauliflower mosaic virus (CaMV) 35S promoter. To generate a binary construct containing *CBR1:sGFP*, the *CBR1:sGFP* fragment was isolated from pUC-CBR1:sGFP by digestion with *Xho*I and *Kpn*I, and inserted into pBIB121(hygromycin) digested with *Xho*I and *Kpn*I.

Generation of Transgenic Plants

The *CBR1:sGFP* binary construct was introduced into *Agrobacterium tumefaciens* by electroporation. Transgenic *Arabidopsis* plants (ecotype Col-0) were generated by the floral dip method (Clough and Bent, 1998). Transgenic plants were selected on Gamborg's B5 plates (Duchefa) containing 50 mg l^{-1} hygromycin. Homozygous plants of the T4 generation were used for all experiments.

Measurement of Chlorophyll a/b Content

Chlorophyll extracts were prepared by treating leaf tissue with 50 volumes of 95% ethanol for 20 min at 80°C. The amount of chlorophyll was calculated as described by Vernon (1960).

qRT–PCR Analysis of Transcripts

Total RNA was prepared from root and shoot tissues using an RNeasy Plant Mini Kit (Qiagen). The cDNA was prepared using a cDNA Reverse Transcription Kit (Biosystems), and qRT–PCR was performed in 20-μl (total volume) reaction mixtures containing 50 ng of cDNA, 10 μl of 2× SYBR Green PCR Master Mix, 200 nM primers, and 1 unit of Taq polymerase. *Actin2* was used as an internal control. The primer sequences are shown in Supplemental Table 1. The PCR conditions were as follows: denaturation at 94°C for 4 min, followed by 35 cycles of 94°C for 15 s, 55°C for 30 s, and 72°C for 60 s.

Preparation of PM Fraction and Vanadate-Sensitive ATPase Activity Measurement

Protoplasts were prepared from 10-day-old plants (Jin et al., 2001), suspended in 5 ml of lysis buffer (0.25 M sucrose, 1 mM EDTA, 20 mM Tris–HCl [pH 7.8]), and gently homogenized by passing through two layers of 11-μm pore nylon filters (Millipore) three times. The extracts were centrifuged at 1000 *g* for 10 min to eliminate large organelles (chloroplasts, mitochondria, and nuclei). The supernatants were placed on top of a 6-ml layer of 30% Percoll in lysis buffer and subjected to centrifugation at 130 000 *g* for 30 min. The PM fraction was collected from the gradient. Percoll was removed from the fraction by diluting with reaction buffer A (30 mM imidazole–HCl [pH 7.5], 50 mM KCl, 4 mM $MgCl_2$, and 0.05% Brij 58), and subjected to ultracentrifugation at 154 000 *g* for 2 h. The pellet (containing PM) was resuspended in reaction buffer A.

ATPase activity was measured in samples containing 10–20 μg of PM proteins by generating inside-out vesicles using Brij 58 (0.05%, Sigma) (Johansson et al., 1995). The activity of vacuolar ATPases was measured in a solution of the same composition but lacking Brij 58. The vanadate-sensitive ATPase activity was computed by subtracting the background signal in reaction buffer B (30 mM imidazole–HCl [pH 7.5], 50 mM KCl, 4 mM $MgCl_2$, 2 mM sodium orthovanadate, and 0.05% Brij 58) from that in reaction buffer A. Sodium orthovanadate stock (100 mM) was prepared following Surowy's method (Surowy and Sussman, 1986). The reaction mixture (1 ml) was incubated on ice for 1 h in the dark. The reaction was started by adding 4 mM Tris–ATP. After 10 min incubation at 23°C, the reaction was stopped by adding 100 μl of 20% SDS. To measure the activity using a colorimetric method (Sarkar, 2002), the reaction mixture (500 μl) was mixed with 500 μl of reagent A (3% ascorbic acid, 0.5 N HCl, and 0.5% ammonium molybdate) and incubated on ice for 10 min to enhance the colors. Subsequently, 500 μl of reagent B (2% sodium meta-arsenite, 2% trisodium citrate, and 2% acetic acid) was added to the reaction, which was incubated at 37°C for 10 min. The activity was measured spectrophotometrically based on the absorbance at 850 nm. A_{850} values were converted to ATPase activity using a standard curve (Supplemental Figure 7A).

Fatty acids (18:0, 18:2, or 18:3; Sigma) were dissolved in 9.6% (v/v) ethanol, 0.1 mM EDTA, 0.1 mM dithiothreitol, and Tris–HCl (pH 8.9) before the addition to reaction buffer A. In the ATPase activity assay, the pH of reaction buffer A was adjusted to 7.5 after the addition of free fatty acids.

Lipid Extraction and Fatty Acid Composition Analysis

Root tissues of 10-day-old seedlings were placed into 2-ml test tubes containing beads. Isopropanol (2 ml) boiled at 80°C was added to the test tubes, and the samples were incubated at 80°C for 10 min on a heating block. The samples were ground three times in a Mixer Mill (MM301; Retsch, Germany) at a frequency of 18 for 2 min, and then decanted into glass tubes. Five hundred seeds were added to 1 ml of boiling isopropanol and heated for 5 min at 80°C. After cooling, 2 ml of chloroform was added to the sample, and the seeds were finely ground with a Polytron homogenizer (Hitachi Koki). Debris was removed by centrifugation at 1600 *g* for 10 min. Lipid extraction was conducted as described previously (Kim et al., 2013). Fatty acid composition was analyzed by gas chromatography–mass spectrometry (Shimadzu GC-2010, HP-INOWAX capillary column, 30 m, 0.25 mm) after acid-catalyzed transmethylation at 90°C for 45 min in 3 ml of 2.5% (v/v) sulfuric acid in methanol.

Electron Microscopy

Dry seeds were fixed in 0.05 M sodium cacodylate buffer (pH 7.2) containing 2% paraformaldehyde and 2% glutaraldehyde at 4°C for 20 h, and washed three times with 0.05 M sodium cacodylate buffer (pH 7.2) at 4°C at 10-min intervals. Post-fixation was performed at 4°C for 2 h with 1% osmium tetroxide in 0.05 M sodium cacodylate buffer (pH 7.2). Samples were dehydrated in a graded ethanol series and embedded using Spurr's resin. Ultrathin sections were prepared using an Ultramicrotome (MT-X; RMC, Tucson, AZ, USA), and stained by treating with 2% uranyl acetate for 7 min followed by treatment with Reynold's lead citrate for 2 min. The sections were observed under a transmission electron microscope (JEM-1011; Jeol, Tokyo, Japan).

Measurement of Element Contents in Plant Seeds and Vegetative Tissues

The element contents were measured in vegetative tissues. Roots and shoots of 10-day-old plants were washed three times with sterile water before use. The tissues were freeze-dried in FreeZone Plus 6 (Labconco), and dry weight was measured. To measure element contents in seeds, 100 seeds were used in each sample. Dried samples were dissolved in 60% HNO_3 at 120°C overnight. After dilution of the nitric acid mixture, the element contents were measured with an inductively coupled plasma mass spectrometer (iCAP6300 DUO ICO-OES; Thermo Electron Corporation).

Measurement of Proton Extrusion from Root Tissues

To measure H^+ efflux, plants were grown for 10 days on 1/2 MS agar plates without sucrose, followed by transfer to 1/2 MS liquid medium containing the pH indicator bromocresol purple (0.005%). One day after the start of incubation, A_{580} of the incubation medium was measured. To visualize rhizosphere acidification, plants were transferred onto 1/2 MS plates (pH 6.5), supplemented with bromocresol blue (0.005%), and grown vertically for 4 days.

Preparation of Protein Extracts and Immunoblot Analysis

Total protein extracts were prepared from plants as described previously (Jin et al., 2001). Protein extracts were separated by SDS–PAGE and analyzed by western blot using anti-AHA2 (Rockland), anti-PIP2, anti-CRT1, anti-CBR1 (Abmart), and anti-ACTIN antibodies as described previously (Jin et al., 2001). The protein blots were developed with an ECL Detection Kit (Amersham Pharmacia Biotech, Piscataway, NJ). Images were obtained using an LAS3000 image capture system (Fujifilm, Tokyo, Japan).

Measurement of ATP Levels

Plants were grown vertically on 1/2 MS plate (pH 5.8) with 1% sucrose for 10 days. ATP levels of root tissues were measured by a luminescent ATP detection assay kit (Abcam) following the manufacturer's instructions.

Measurement of Fe(III) Chelate Reductase Activity

Two-week-old seedlings grown on 1/2 MS containing 1% sucrose in the presence or absence of 300 μM Ferrozine were used to measure Fe(III) chelate reductase activity. Roots of seedlings were completely submerged in 0.1 mM Fe(III)–EDTA and 0.3 mM Ferrozine solution for 20 min at room temperature without light. After incubation, the amount of purple-colored Fe(II)–Ferrozine complexes was measured by absorbance at 562 nm. The concentration of Fe(II)–Ferrozine complex was analyzed using a molar extinction coefficient of 28.6 mM^{-1} cm^{-1} (Gibbs, 1976).

SUPPLEMENTAL INFORMATION

Supplemental Information is available at *Molecular Plant Online*.

FUNDING

This research was supported by a grant from the National Research Foundation of the Ministry of Education, Science and Technology (Korea) (R31-2008-000-10105-0).

AUTHOR CONTRIBUTIONS

Y.J.O. and I.H. designed the experiments. Y.J.O. performed most of the phenotype analysis of *CBR1*-OX and *cbr1-2* mutant plants. Y.J.O., H.K., and Y.L. performed lipid extraction and data analysis. S.H.S. and Y.S.C. performed the element content measurements in plants using inductively coupled plasma spectrometry. D.W.L., J.H.L., E.J.S., B.G.H., and S.J.L. performed experiments. Y.J.O. and I.H. analyzed the data and wrote the paper.

ACKNOWLEDGMENTS

We thank John Browse, Washington State University, Pullman, WA, USA for providing *fad2-1* and *fad3-2* mutant seeds. No conflict of interest declared.

Received: September 29, 2015
Revised: November 23, 2015
Accepted: December 7, 2015
Published: December 19, 2015

REFERENCES

Bernardi, P., and Azzone, G.F. (1981). Cytochrome c as an electron shuttle between the outer and inner mitochondrial membranes. J. Biol. Chem. **256**:7187–7192.

Bocca, A., Di Fava, R.C., and Gaudiano, A. (1984). Bioavailability from foods of trace elements: iron, zinc, copper, selenium, chromium, lead, cadmium, mercury. Ann. Ist. Super. Sanita **20**:149–169.

Browse, J., McConn, M., James, D., and Miquel, M. (1993). Mutants of *Arabidopsis* deficient in the synthesis of α-linolenate. J. Biol. Chem. **268**:16345–16351.

Chen, M., and Thelen, J.J. (2013). *ACYL-LIPID DESATURASE2* is required for chilling and freezing tolerance in *Arabidopsis*. Plant Cell **25**:1430–1444.

Clemens, S. (2001). Molecular mechanisms of plant metal tolerance and homeostasis. Planta **212**:475–486.

Clough, S.J., and Bent, A.F. (1998). Floral dip: a simplified method for *Agrobacterium*-mediated transformation of *Arabidopsis thaliana*. Plant J. **16**:735–743.

Colangelo, E.P., and Guerinot, M.L. (2004). The essential basic helix-loop-helix protein FIT1 is required for the iron deficiency response. Plant Cell **16**:3400–3412.

Connolly, E.L., Campbell, N.H., Grotz, N., Prichard, C.L., and Guerinot, M.L. (2003). Overexpression of the FRO2 ferric chelate reductase confers tolerance to growth on low iron and uncovers posttranscriptional control. Plant Physiol. **133**:1102–1110.

Curie, C., Alonso, J.M., Le Jean, M., Ecker, J.R., and Briat, J.F. (2000). Involvement of NRAMP1 from *Arabidopsis thaliana* in iron transport. Biochem. J. **347**:749–755.

Eide, D., Broderius, M., Fett, J., and Guerinot, M.L. (1996). A novel iron-regulated metal transporter from plants identified by functional expression in yeast. Proc. Natl. Acad. Sci. USA **93**:5624–5628.

Gibbs, C.R. (1976). Characterization and application of FerroZine iron reagent as a ferrous iron indicator. Anal. Chem. **48**:1197–1201.

Giehl, R., Lima, J., and von Wiren, N. (2012). Localized iron supply triggers lateral root elongation in *Arabidopsis* by altering the AUX1-mediated auxin distribution. Plant Cell **24**:33–49.

Hänsch, R., and Mendel, R.R. (2009). Physiological functions of mineral micronutrients (Cu, Zn, Mn, Fe, Ni, Mo, B, Cl). Curr. Opin. Plant Biol. **12**:259–266.

Heazlewood, J.L., Tonti-Filippini, J.S., Gout, A.M., Day, D.A., Whelan, J., and Millar, A.H. (2004). Experimental analysis of the *Arabidopsis* mitochondrial proteome highlights signaling and regulatory components, provides assessment of targeting prediction programs,

and indicates plant-specific mitochondrial proteins. Plant Cell **16**:241–256.

Hernandez, H., and Cooke, D. (1997). Modification of the root plasma membrane lipid composition of cadmium-treated *Pisum sativum*. J. Exp. Bot. **48**:1375–1381.

Jahn, T., Fuglsang, A.T., Olsson, A., Brüntrup, I.M., Collinge, D.B., Volkmann, D., Sommarin, M., Palmgren, M.G., and Larsson, C. (1997). The 14-3-3 protein interacts directly with the C-terminal region of the plant plasma membrane H^+-ATPase. Plant Cell **9**:1805–1814.

Jin, J.B., Kim, Y.A., Kim, S.J., Lee, S.H., Kim, D.H., Cheong, G.W., and Hwang, I. (2001). A new dynamin-like protein, ADL6, is involved in trafficking from the trans-Golgi network to the central vacuole in *Arabidopsis*. Plant Cell **13**:1511–1526.

Johansson, F., Olbe, M., Sommarin, M., and Larsson, C. (1995). Brij 58, a polyoxyethylene acyl ether, creates membrane vesicles of uniform sidedness. A new tool to obtain inside-out (cytoplasmic side-out) plasma membrane vesicles. Plant J. **7**:165–173.

Kaplan, M.R., and Simoni, R.D. (1985). Intracellular transport of phosphatidylcholine to the plasma membrane. J. Cell Biol. **101**: 441–445.

Kim, S., Yamaoka, Y., Ono, H., Kim, H., Shim, D., Maeshima, M., Martinoia, E., Cahoon, E.B., Nishida, I., and Lee, Y. (2013). AtABCA9 transporter supplies fatty acids for lipid synthesis to the endoplasmic reticulum. Proc. Natl. Acad. Sci. USA **110**:773–778.

Kodama, H., Hamada, T., Horiguchi, G., Nishimura, M., and Iba, K. (1994). Genetic enhancement of cold tolerance by expression of a gene for chloroplast ω-3 fatty acid desaturase in transgenic tobacco. Plant Physiol. **105**:601–605.

Kumar, R., Wallis, J.G., Skidmore, C., and Browse, J. (2006). A mutation in *Arabidopsis* cytochrome b5 reductase identified by high-throughput screening differentially affects hydroxylation and desaturation. Plant J. **48**:920–932.

Lanquar, V., Lelievre, F., Bolte, S., Hames, C., Alcon, C., Neumann, D., Vansuyt, G., Curie, C., Schroder, A., Kramer, U., et al. (2005). Mobilization of vacuolar iron by AtNRAMP3 and AtNRAMP4 is essential for seed germination on low iron. EMBO J. **24**:4041–4051.

Lee, S., Jeon, J.S., and An, G. (2012). Iron homeostasis and fortification in rice. J. Plant Biol. **55**:261–276.

Lopez-Villalobos, A., Dodds, P., and Hornung, R. (2001). Changes in fatty acid composition during development of tissues of coconut (*Cocos nucifera* L.) embryos in the intack nut and *in vitro*. J. Exp. Bot. **52**:933–942.

Miquel, M., and Browse, J. (1992). *Arabidopsis* mutants deficient in polyunsaturated fatty acid synthesis. Biochemical and genetic characterization of a plant oleoyl-phosphatidylcholine desaturase. J. Biol. Chem. **267**:1502–1509.

Palmgren, M.G., Sommarin, M., Ulvskov, P., and Jorgensen, P.L. (1988). Modulation of plasma membrane H^+-ATPase from oat roots by lysophosphatidylcholine, free fatty acids and phospholipase A2. Physiol. Plant. **74**:11–19.

Palmgren, M.G., Sommarin, M., Ulvskov, P., and Larsson, C. (1990). Effect of detergents on the H^+-ATPase activity of inside-out and right-side-out plant plasma membrane vesicles. Biochim. Biophys. Acta **1021**:133–140.

Percy, M.J., and Lappin, T.R. (2008). Recessive congenital methaemoglobinaemia: cytochrome b(5) reductase deficiency. Br. J. Haematol. **141**:298–308.

Pilon, M., Cohu, C.M., Ravet, K., Abdel-Ghany, S.E., and Gaymard, F. (2009). Essential transition metal homeostasis in plants. Curr. Opin. Plant Biol. **12**:347–357.

Pineau, C., Loubet, S., Lefoulon, C., Chalies, C., Fizames, C., Lacombe, B., Ferrand, M., Loudet, O., Berthomieu, P., and Richard, O. (2012). Natural variation at the FRD3 MATE transporter locus reveals cross-talk between Fe homeostasis and Zn tolerance in *Arabidopsis thaliana*. Plos Genet. **8**:e1003120.

Regvar, M., Eichert, D., Kaulich, B., Gianoncelli, A., Pongrac, P., Vogel-Mikus, K., and Kreft, I. (2011). New insights into globoids of protein storage vacuoles in wheat aleurone using synchrotron soft X-ray microscopy. J. Exp. Bot. **62**:3929–3939.

Robinson, N.J., Procter, C.M., Connolly, E.L., and Guerinot, M.L. (1999). A ferric-chelate reductase for iron uptake from soils. Nature **397**:694–697.

Santi, S., and Schmidt, W. (2009). Dissecting iron deficiency-induced proton extrusion in *Arabidopsis* roots. New Phytol. **183**:1072–1084.

Sarkar, P.K. (2002). A quick assay for Na^+-K^+-ATPase specific activity. Z. Naturforsch. C **57**:562–564.

Shanmugam, V., Lo, J.C., Wu, C.L., Wang, S.L., Lai, C.C., Connolly, E.L., Huang, J.L., and Yeh, K.C. (2011). Differential expression and regulation of iron-regulated metal transporters in *Arabidopsis halleri* and *Arabidopsis thaliana* the role in zinc tolerance. New Phytol. **190**:125–137.

Sinclair, S.A., and Kramer, U. (2012). The zinc homeostasis network of land plants. Biochim. Biophys. Acta **1823**:1553–1567.

Surowy, T.K., and Sussman, M.R. (1986). Immunological cross-reactivity and inhibitor sensitivities of the plasmamembrane H^+-ATPase from plants and fungi. Biochim. Biophys. Acta **848**:24–34.

Sze, H., Li, X., and Palmgren, M.G. (1999). Energization of plant cell membranes by H^+-pumping ATPases. Regulation and biosynthesis. Plant Cell **11**:677–690.

Threntham, D.R. (1971). Reactions of D-glyceraldehyde 3-phosphate dehydrogenase facilitated by oxidized nicotinamide-adenine dinucleotide. J. Biol. Chem. **122**:59–69.

Vernon, L.P. (1960). Spectrophotometric determination of chlorophylls and pheophytins in plant extracts. Anal. Chem. **32**:1144–1150.

Vert, G., Grotz, N., Dedaldechamp, F., Gaymard, F., Guerinot, M.L., Briat, J.F., and Curie, C. (2002). IRT1, an *Arabidopsis* transporter essential for iron uptake from the soil and for plant growth. Plant Cell **14**:1223–1233.

Walker, E.L., and Waters, B.M. (2011). The role of transition metal homeostasis in plant seed development. Curr. Opin. Plant Biol. **14**:318–324.

Wayne, L.L., Wallis, J.G., Kumar, R., Markham, J.E., and Browse, J. (2013). Cytochrome b5 reductase encoded by CBR1 is essential for a functional male gametophyte in *Arabidopsis*. Plant Cell **25**:3052–3066.

Yi, Y., and Guerinot, M.L. (1996). Genetic evidence that induction of root Fe(III) chelate reductase activity is necessary for iron uptake under iron deficiency. Plant J. **10**:835–844.